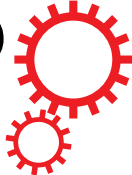


SCIENTIFIC REPORTS



OPEN

Enhanced Thermal Conductivity and Dielectric Properties of Iron Oxide/Polyethylene Nanocomposites Induced by a Magnetic Field

Qingguo Chi^{1,2,3}, Tao Ma^{1,2}, Jiufeng Dong^{1,2}, Yang Cui¹, Yue Zhang¹, Changhai Zhang¹, Shichong Xu⁴, Xuan Wang¹ & Qingquan Lei¹

Iron Oxide (Fe_3O_4) nanoparticles were deposited on the surface of low density polyethylene (LDPE) particles by solvothermal method. A magnetic field was introduced to the preparation of Fe_3O_4 /LDPE composites, and the influences of the magnetic field on thermal conductivity and dielectric properties of composites were investigated systematically. The Fe_3O_4 /LDPE composites treated by a vertical direction magnetic field exhibited a high thermal conductivity and a large dielectric constant at low filler loading. The enhancement of thermal conductivity and dielectric constant is attributed to the formation of the conductive chains of Fe_3O_4 in LDPE matrix under the action of the magnetic field, which can effectively enhance the heat flux and interfacial polarization of the Fe_3O_4 /LDPE composites. Moreover, the relatively low dielectric loss and low conductivity achieved are attributed to the low volume fraction of fillers and excellent compatibility between Fe_3O_4 and LDPE. Of particular note is the dielectric properties of Fe_3O_4 /LDPE composites induced by the magnetic field also retain good stability across a wide temperature range, and this contributes to the stability and lifespan of polymer capacitors. All the above-mentioned properties along with the simplicity and scalability of the preparation for the polymer nanocomposites make them promising for the electronics industry.

Owing to the rapid developments in modern science and technology, the capacitors with remarkable performance were urgently required in the field of electronics and electrical systems. Nowadays, outstanding-performance polymers, which possess a high dielectric constant and flexibility, but low dielectric loss, have attracted great attention owing to their potential application in many cutting-edge industries, including microelectronics, aerospace, and aviation^{1–3}. In general, the polymers possess excellent flexibility and high breakdown strength, but their applications were limited by their low dielectric constant^{4,5}. The organic-inorganic hybrid strategy, including ceramic/polymer and conductive fillers/polymer composites have been widely adopted^{6–10}. Unfortunately, the ceramic/polymer composites have a limited dielectric constant and often require a large filler loading (>60 vol.%), which causes poor flexibility and uniformity of the materials. The conductive fillers/polymer composites can exhibit very high dielectric constant, but with a relatively high dielectric loss due to the insulator-conductor transition near the percolation threshold, which significantly restricts its practical application.

With the miniaturization of microelectronics and associated increase in power densities, the internal thermal stability of integrated microelectronic devices has become one of the critical factors in achieving advanced performance and extended lifespan^{11–13}. It is crucial for the heat generated from electronics to be dissipated as quickly and effectively as possible, which can maintain the operating temperatures of the electronic equipment

¹Key Laboratory of Engineering Dielectrics and Its Application, Ministry of Education, Harbin University of Science and Technology, Harbin, 150080, P.R. China. ²School of Applied Science, Harbin University of Science and Technology, Harbin, 150080, P.R. China. ³State Key Laboratory of Electronic Thin Films and Integrated Devices, University of Electronic Science and Technology of China, Chengdu, 610054, P.R. China. ⁴Key Laboratory of Functional Materials Physics and Chemistry of the Ministry of Education, Jilin Normal University, Siping, 136000, P.R. China. Correspondence and requests for materials should be addressed to Q.C. (email: qgchi@hotmail.com)

at a desired level, because the dielectric strength will decrease with increasing temperature owing to the poor thermal conduction of these dielectric materials. Notably, traditional high dielectric composites would lose their electromechanical stability and displayed a large variation in dielectric constant as well as dielectric loss at a broad temperature range, hindering their reliability and efficiency¹⁴.

Previous studies have shown that the polymeric composites, which were integrated with high thermal conductivity fillers, such as metal (Cu)¹⁵, oxide (Al₂O₃)¹⁶, aluminum nitride (AlN)¹⁷, carbide (SiC)¹⁸, and carbon nanotubes¹⁹, can endow themselves with superior properties. For example, Cu-filled low-density polyethylene (LDPE) composites were studied by Luyt *et al.*¹⁵ and they found that the thermal conductivity of the composites was 0.35 W m⁻¹ K⁻¹ when the volume fraction of the Cu particles was 7.0 vol.%. Fang *et al.*¹⁸ prepared different dimensional SiC particles to be filled into LDPE composites, and realized that the thermal conductivity of the composites was 0.37 W m⁻¹ K⁻¹ at 10 vol.% SiC content. High thermal conductivity of the composites usually requires a high volume fraction of fillers, and provision of a low dielectric constant, which is not suitable for use for microelectronics. Additionally, most research has just focused on one single side of thermal conductivity or dielectric property of nanocomposites at room temperature. Few in-depth explorations of the cooperative effect of a large thermal conductivity and a high dielectric constant for polymer materials under broader temperature conditions have been investigated until now, and their influential mechanism is still uncertain. Beyond that, how to improve the thermal conductivity and the dielectric performance of composites at low filler loading is one of the key issues.

The external electric and magnetic field could significantly influence the polymer's molecular arrangement and the conductive particles' distribution of the polymer composites, in the end the microstructure and macro-properties of the composites are influenced^{20–22}. Hence, in this research, the Fe₃O₄-LDPE particles were prepared by solvothermal reaction and then the surface was modified by polydopamine (PDA). On this basis, we treated the Fe₃O₄/LDPE composites under a constant magnetic field for 30 min at 130 °C. Henceforth, the composites of Fe₃O₄/LDPE treated by the magnetic field can be abbreviated as M-Fe₃O₄/LDPE, here, "M" means that there has been magnet field treatment applied on the samples. The influence of the external magnetic field on the dielectric properties and thermal conductivity of Fe₃O₄/LDPE composites were studied intensively. It can be found that the orientation of the Fe₃O₄ nanoparticles was remote controlled by the external magnetic field because of its ultra-high magnetic response. Compared with the Fe₃O₄/LDPE composites, the M-Fe₃O₄/LDPE composites exhibit higher thermal conductivity and dielectric properties at 7.0 vol.% concentration, and the relevant mechanisms are discussed in detail.

Results and Discussion

Morphology of Fe₃O₄-LDPE particles and LDPE composites. The morphology of the Fe₃O₄-LDPE particles is directly illustrated by scanning electron microscope (SEM) images, as shown in Fig. 1a. The LDPE particles have a non-spherical shape and with an average diameter of about 90 μm, and the Fe₃O₄ nanoparticles are uniformly deposited on LDPE particles. Figure 1b shows the X-ray diffraction (XRD) curves of the Fe₃O₄/LDPE composites with 7.0 vol.% Fe₃O₄ fillers. The characteristic diffraction peaks of Fe₃O₄ appear at 2θ = 30.18°, 35.56°, 43.24°, 53.54°, 57.10°, and 62.47°, corresponding to the diffraction peaks from (220), (311), (440), (422), (511), and (440), respectively. The XRD patterns of the composites clearly indicate that the Fe₃O₄ particles filled the polymer matrix.

The SEM image of the freeze-fractured cross-sections of the LDPE-based composite films containing 7 vol.% Fe₃O₄ nanoparticles is displayed in Fig. 1c. The Fe₃O₄ nanoparticles with an the average size of about 90 nm are embedded in the LDPE matrix without agglomeration, and there is no evidence of defects and voids in the Fe₃O₄/LDPE composites, which is due to the solvothermal reaction process of the Fe₃O₄-LDPE particles lowering the probability of the agglomeration of the Fe₃O₄ nanoparticles. The surfactant treatment of PDA greatly improved the compatibility of the Fe₃O₄ nanoparticles and LDPE matrix²³. Figure 1d shows the SEM morphology of the fractured cross-surface of M-Fe₃O₄/LDPE composite at 7 vol.% concentration. It is clearly found that some Fe₃O₄ particles come into contact with each other and become short chains along the magnetic direction. That is, the distribution of the Fe₃O₄ particles in the LDPE matrix is changed and the chains of the Fe₃O₄ particles are formed under the action of the magnetic field.

Thermal conductivity of Fe₃O₄/LDPE composites and M-Fe₃O₄/LDPE composites. In this research, the Fe₃O₄-LDPE particles were prepared via a solvothermal reaction before preparing the Fe₃O₄/LDPE composites. To highlight the advantages of this method, the comparison of the thermal conductivity of the Fe₃O₄/LDPE composites prepared by a simple mixing method and solvothermal reaction is shown in Fig. 2. Compared with the simple mixing method, the Fe₃O₄/LDPE composites prepared by solvothermal reaction show a higher thermal conductivity at the same filler content. For instance, the maximum thermal conductivity of the Fe₃O₄/LDPE composites via the solvothermal reaction is 0.384 W m⁻¹ K⁻¹ at 7.0 vol.% concentration, higher than that of Fe₃O₄/LDPE composites prepared by a simple mixing method (0.350 W m⁻¹ K⁻¹). As shown in the inset of Fig. 2, the voiding occurs due to the agglomeration and the weak compatibility of the Fe₃O₄ nanoparticles and LDPE matrix prepared by the simple mixing method, which leads to poor thermal conductivity of the Fe₃O₄/LDPE composites. This also indicated that the solvothermal treatment could effectively improve the dispersion of the Fe₃O₄ nanoparticles in the LDPE matrix.

The curves of thermal conductivity of the composites versus filler content are displayed in Fig. 3. All of the composites show an enhancement in thermal conductivity with increasing Fe₃O₄ concentration. Moreover, a non-linear increase in thermal conductivity is also observed. The higher thermal conductivity of the composites should result from the higher intrinsic thermal conductivity of the Fe₃O₄ particles in comparison with the LDPE matrix^{24,25}. Importantly, the thermal conductivity of the M-Fe₃O₄/LDPE composites are much higher than that of the Fe₃O₄/LDPE composites at the same loading. For instance, the thermal conductivity of the M-Fe₃O₄/

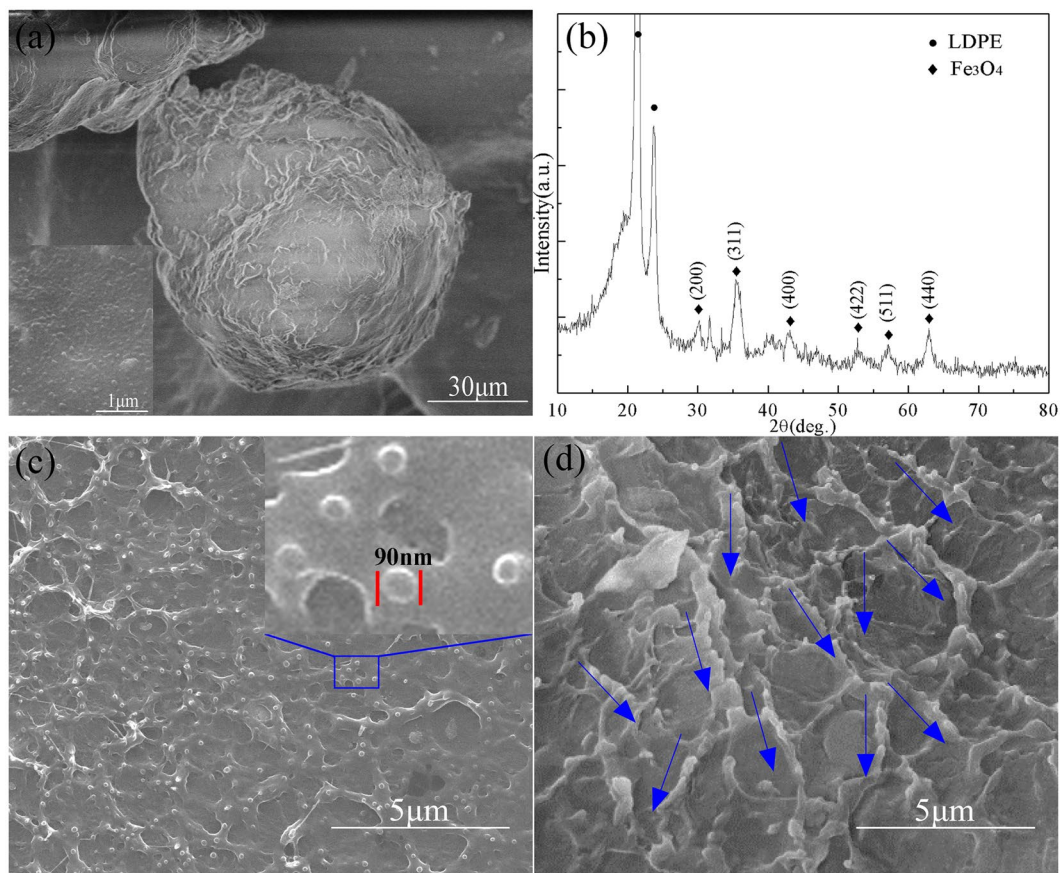


Figure 1. (a) SEM images of the Fe_3O_4 -LDPE particles. The inset shows the partial SEM image of the Fe_3O_4 -LDPE particles. (b) XRD pattern of the Fe_3O_4 /LDPE composites at 7 vol.% concentration. (c) Cross-sectional SEM images of the Fe_3O_4 /LDPE composites at 7 vol.% concentration. The inset shows the partial SEM image of the Fe_3O_4 /LDPE composites. (d) Cross-sectional SEM images of the M- Fe_3O_4 /LDPE composites at 7 vol.% concentration.

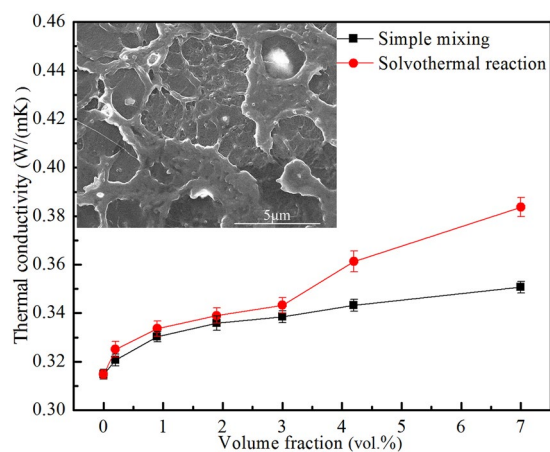


Figure 2. Comparison of thermal conductivity of Fe_3O_4 /LDPE composites prepared by simple mixing method and solvothermal reaction. The inset shows the cross-sectional SEM images of the Fe_3O_4 /LDPE composites at 7 vol.% concentration prepared by simple mixing method.

LDPE composites is $0.461 \text{ W m}^{-1} \text{ K}^{-1}$ at 7.0 vol.% concentration, higher than that of the Fe_3O_4 /LDPE composites ($0.384 \text{ W m}^{-1} \text{ K}^{-1}$), and this value is superior to that of many previous reports^{15, 18, 20, 26–28}. As shown in Table 1, the thermal conductivity of our composites is larger than that of the high-density polyethylene/fly-ash (HDPE/

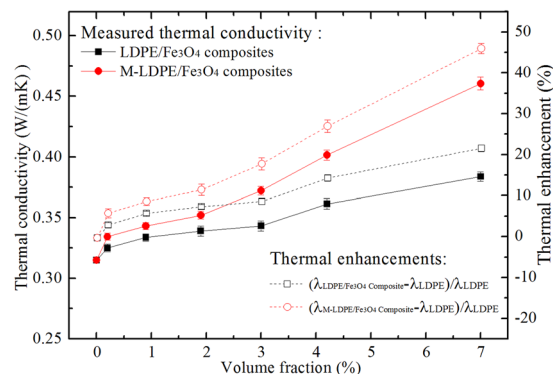


Figure 3. Thermal conductivity of the $\text{Fe}_3\text{O}_4/\text{LDPE}$ and $\text{M-Fe}_3\text{O}_4/\text{LDPE}$ composites corresponding to thermal enhancements.

Composites	λ (w/mk)	f (vol.%)	Ref.
$\text{Fe}_3\text{O}_4/\text{LDPE}$	0.384	7	Our work
$\text{M-Fe}_3\text{O}_4/\text{LDPE}$	0.461	7	Our work
LDPE-Cu	0.35	7	[15]
$\text{SiC (21 }\mu\text{m)/LLDPE}$	0.52	≈ 10.77	[18]
Rmh-BN-Silicone	0.349	7.5	[20]
AlN (A-100)/HDPE	0.46	10	[26]
HDPE/FA	≈ 0.41	10	[27]
AlN/Polyimide	0.75	32	[28]

Table 1. Comparison of the thermal conductivity of our composites and reported literature materials.

FA) composites containing 10 vol.% FA ($\approx 0.41 \text{ W m}^{-1} \text{ K}^{-1}$)²⁷. It should be pointed out that the filler content of the $\text{M-Fe}_3\text{O}_4/\text{LDPE}$ composites is smaller than that of other literature materials, with better flexibility.

Figure 3 also presents the thermal enhancements of the $\text{Fe}_3\text{O}_4/\text{LDPE}$ and $\text{M-Fe}_3\text{O}_4/\text{LDPE}$ composites with pure LDPE, respectively. Herein, the thermal enhancement is defined as the percentage of thermal conductivity improvement by Fe_3O_4 ^{20,29}. It can be found that the thermal enhancement of the $\text{Fe}_3\text{O}_4/\text{LDPE}$ and $\text{M-Fe}_3\text{O}_4/\text{LDPE}$ composites increases initially with the filler content, reaching 21.88% and 46.27% at 7.0 vol.% concentration, respectively. The $\text{M-Fe}_3\text{O}_4/\text{LDPE}$ composites show a better heat conduction effect than the $\text{Fe}_3\text{O}_4/\text{LDPE}$ composites, owing to the formation of efficient thermal pathways made by the Fe_3O_4 oriented parallel to the heat flux under the action of the magnetic field (see Fig. 1d).

To further explore the thermal conductivity behavior of the $\text{Fe}_3\text{O}_4/\text{LDPE}$ and $\text{M-Fe}_3\text{O}_4/\text{LDPE}$ composites, Maxwell-Eucken's model has been proposed and the comparisons between the experimental and theoretical values were made³⁰. Maxwell-Eucken assumes that filler particles are homogeneously distributed in the polymer matrix, non-interacting, and roughly spherical. Fewer filler particles would be covered by the polymer and dispersed in the form of isolated islands in the matrix:

$$\lambda_c = \frac{2\lambda_p + \lambda_f + 2V_f(\lambda_f - \lambda_p)}{2\lambda_p + \lambda_f - 2V_f(\lambda_f - \lambda_p)}\lambda_p \quad (1)$$

where V_f is the volume fraction of the filler, and λ_c , λ_f and λ_p is the thermal conductivity of composites, filler, and matrix, respectively^{31,32}. In this paper, the value of λ_f and λ_p used $6.032 \text{ W m}^{-1} \text{ K}^{-1}$ and $0.315 \text{ W m}^{-1} \text{ K}^{-1}$, respectively.

Figure 4 gives the comparison between the experimental data and the thermal conductivity predicted by the Maxwell-Eucken's model of the composites. For the $\text{Fe}_3\text{O}_4/\text{LDPE}$ composites, Fe_3O_4 nanoparticles are dispersed randomly in the $\text{Fe}_3\text{O}_4/\text{LDPE}$ composites (shown in Fig. 1c), and the theoretical values match well with the experimental data. However, it is interesting to note that the theoretical values of the $\text{M-Fe}_3\text{O}_4/\text{LDPE}$ composites are lower than those observed in the experiments. This deviation could be attributed to the easier formation of the thermal conductive net-chain by the interaction of Fe_3O_4 in the LDPE matrix under the action of the magnetic field.

Owing to the Maxwell-Eucken model not matching well with the $\text{M-Fe}_3\text{O}_4/\text{LDPE}$ composites, two heat conduction models (parallel and vertical models) were brought forward to judge the heat flow direction in the polymer composites, based on the formation of the thermal conductive net-chain and mutual interaction of particles^{33,34}. Considering the crystallinity of the filler and polymer, Agari's model was created based on a hypothesis of homogeneous dispersion of particles in the polymer:

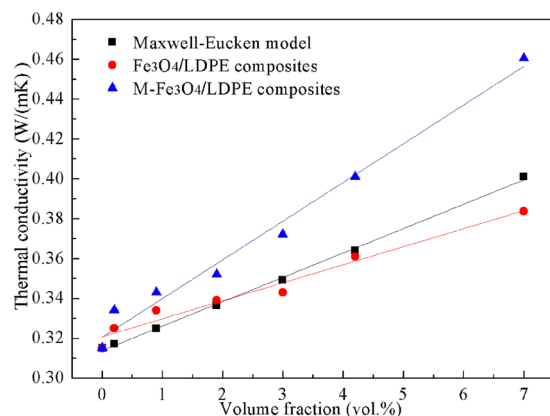


Figure 4. Thermal conductivity of the Fe₃O₄/LDPE and M-Fe₃O₄/LDPE composites based on experimental data and Maxwell-Eucken's model.

Composites	A	B	C _p	C _f	R ²
Fe ₃ O ₄ /LDPE	1.11624	-0.55891	1.02028	0.87656	0.96233
M-Fe ₃ O ₄ /LDPE	2.19564	-0.49094	1.02505	1.72694	0.98522

Table 2. Values of C_p and C_f for the Fe₃O₄/LDPE and M-Fe₃O₄/LDPE composites.

$$\log \lambda = VC_2 \log \lambda_f + (1 - V)\log(\lambda_p C_1) \quad (2)$$

where C₁ is the constant, which is related to the crystallinity and crystalline dimension of a polymer, and C₂ is the free factor, which indicates the ability of forming a heat conductive net-chain for fillers. C₂ would significant change due to the increase of the particle filling; therefore, Agari's model should be modified and verified as the following^{32, 35}:

$$\log \lambda = C_f V \log[\lambda_f / (C_p \lambda_p)] + \log(C_p \lambda_p) = AV + B \quad (3)$$

where C_p is the formation of the thermal conductive chain free particles, and C_f is the reflecting particle formation of the thermal conductivity of difficulty.

Table 2 shows the C_p and C_f for the above two composites. It can be found that the C_p of the M-Fe₃O₄/LDPE composites did not change significantly compared with the Fe₃O₄/LDPE composites. However, the C_f of the M-Fe₃O₄/LDPE composites was greater than that of the Fe₃O₄/LDPE composites. The factor C_f related to the ease in forming conductive chains of the filler, that is, the magnetic field shows a strong effect on C_f. This also indicates that the external magnetic field could effectively enhance the formation of thermal conductive paths in the LDPE matrix, which is consistent with the results shown in Fig. 1d. In addition, R² stands for the fitting degree between the theoretical data and the experimental data. The R² value of the M-Fe₃O₄/LDPE composites is 0.98522, higher than that of the Fe₃O₄/LDPE composites (0.96233), showing that the experimental results for the M-Fe₃O₄/LDPE composites had a better fitting effect than the Fe₃O₄/LDPE composites. Besides, as shown in Fig. 1d, some changes have taken place in the structure of the LDPE matrix. This phenomenon also indicated that the external magnetic field has some influence on the microstructure of polymer matrix, the similar result has been reported in numerous previous studies^{36–38}. It may be one of the reasons for the thermal conductivity enhancement of M-Fe₃O₄/LDPE composites.

Dielectric properties of Fe₃O₄/LDPE composites and M-Fe₃O₄/LDPE composites. The thermal conductivity of the Fe₃O₄/LDPE composites is enhanced by the formation of conductive chains of the Fe₃O₄ filler under the action of the magnetic field. Moreover, the distribution of the Fe₃O₄ nanoparticles also affects the dielectric properties of the corresponding materials. Figure 5 shows the dependence of volume fraction and dielectric properties of the Fe₃O₄/LDPE and M-Fe₃O₄/LDPE composites at 10 Hz and room temperature. It can be found that the dielectric constant of the composites increases with gradually increasing filler content. The maximum dielectric constant of the Fe₃O₄/LDPE composites is 4.45 when the content of Fe₃O₄ is 7.0 vol.%. In comparison with pure LDPE (ε = 2.3), the dielectric constant of the composite is nearly 2 times higher. This demonstrates that incorporating conducting fillers into the polymer matrix results in an increase in dielectric constant. Moreover, the dielectric constant of the M-Fe₃O₄/LDPE is higher than the Fe₃O₄/LDPE composites at the same concentration. In particular, the dielectric constant of the M-Fe₃O₄/LDPE composites reaches 51 at 7.0 vol.% concentration, which is 11.6 times higher than that of the Fe₃O₄/LDPE composites. Fe₃O₄ nanoparticles are able to move easily and touch together to form clusters in a melting state of the polymer matrix (at 130 °C), and these clusters would array in parallel along the direction of the magnetic field^{21, 22}. The oriented distribution of the Fe₃O₄ clusters is beneficial for the formation of a conductive network in this direction, which can be

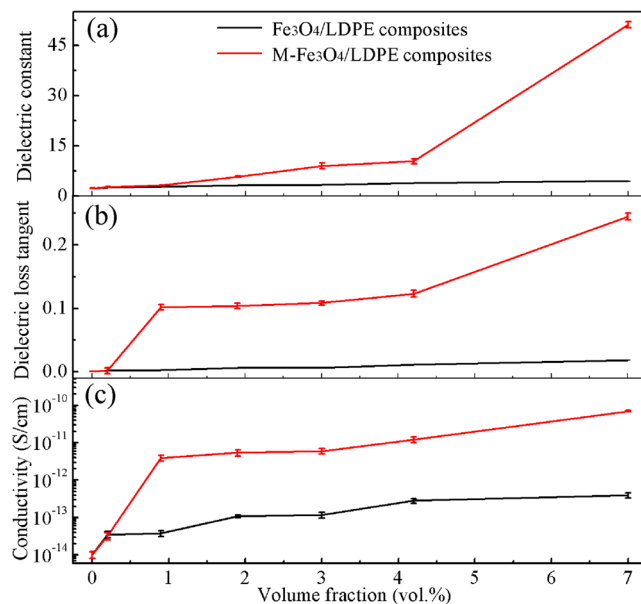


Figure 5. (a) Dielectric constant (b) dielectric loss tangent and (c) conductivity of the $\text{Fe}_3\text{O}_4/\text{LDPE}$ and $\text{M-Fe}_3\text{O}_4/\text{LDPE}$ composites at different volume fraction of Fe_3O_4 filler at 10 Hz.

Composites	ϵ	$\tan \delta$	σ (S/cm)	f (vol.%)	Ref.
$\text{Fe}_3\text{O}_4/\text{LDPE}$	4.45	0.0188	3.96×10^{-13}	7	Our work
$\text{M-Fe}_3\text{O}_4/\text{LDPE}$	51	0.25	7×10^{-11}	7	Our work
PVDF/Ni	45	0.2	—	5	[21]
P(VDF-HFP)/BT-PDA-Ag	≈ 44	0.213	—	20	[23]
BZT-BCT/PVDF	37.2	0.08	1.5×10^{-9}	24	[41]
$\text{Fe}_3\text{O}_4/\text{SiO}_2/\text{BECy}$	9.5	0.09	—	20	[42]
PEG- Fe_3O_4 /PVDF	≈ 80	≈ 1.25	$\approx 7.0 \times 10^{-9}$	7.5	[43]

Table 3. Comparison of the dielectric properties of our composites and reported literature materials.

regarded as a great amount of parallel-connected micro-capacitors, resulting in a greatly enhanced dielectric constant^{39,40}. It should be noted that the dielectric properties in our present study is even higher than those of many previous reports^{21,23,41–43}. For example, as shown in Table 3, the obtained dielectric constant is higher than that of BZT-BCT/PVDF composites containing 24 vol.% BZT-BCT ($\epsilon = 37.2$ at 10 Hz)⁴¹. Moreover, the amount of filler in the $\text{M-Fe}_3\text{O}_4/\text{LDPE}$ composites is smaller than that in other materials described in the literature, and displayed better flexibility. For embedded capacitor applications, the dielectric loss is an essential parameter. The dielectric loss measured at a certain frequency includes polarization loss and conduction loss⁴⁴. The dielectric loss tangent for the $\text{M-Fe}_3\text{O}_4/\text{LDPE}$ composites remain below 0.25 at 10 Hz, and the conductivity of the $\text{M-Fe}_3\text{O}_4/\text{LDPE}$ composites is also kept at a low value (7×10^{-11} S/cm). These attributed to the improvement of the interfacial adhesion and compatibility between the filler and the matrix by surface treatment of the PDA, no complete conducting path was formed in the composites (shown in Fig. 1d), resulting in a low dielectric loss and low conductivity of the composites within the acceptable ranges⁴⁵. For example, the achieved dielectric loss and conductivity were found to be significant smaller than that of PEG- Fe_3O_4 /PVDF composites containing 7.5 vol.% PEG- Fe_3O_4 fillers⁴³.

In addition to the movement of particles under the magnetic field, the dielectric relaxation is also likely to affect the dielectric properties. To clarify the mechanism of the dielectric behaviors of the $\text{Fe}_3\text{O}_4/\text{LDPE}$ and $\text{M-Fe}_3\text{O}_4/\text{LDPE}$ composites, an electric modulus formalism based analysis of the dielectric relaxation in the composites has been proposed. Complex dielectric modulus formalism M^* is demonstrated as follows:^{46,47}

$$M^* = \frac{1}{\epsilon^*} = \frac{1}{\epsilon' - j\epsilon''} = \frac{\epsilon'}{\epsilon'^2 + \epsilon''^2} + j \frac{\epsilon''}{\epsilon'^2 + \epsilon''^2} = M' + jM'' \quad (4)$$

where M' is the real and M'' the imaginary part of the electric modulus, respectively. The imaginary part M'' of the electric modulus takes the form of loss curves, allowing us to interpret the relaxation phenomena.

The frequency dependence of M' and M'' for the $\text{Fe}_3\text{O}_4/\text{LDPE}$ and $\text{M-Fe}_3\text{O}_4/\text{LDPE}$ composites is shown in Fig. 6. The change regularity of the $\text{Fe}_3\text{O}_4/\text{LDPE}$ composites is insignificant with the increasing of Fe_3O_4 content (Fig. 6a). However, for the $\text{M-Fe}_3\text{O}_4/\text{LDPE}$ composites, it can be seen that M' decreases with the increasing of

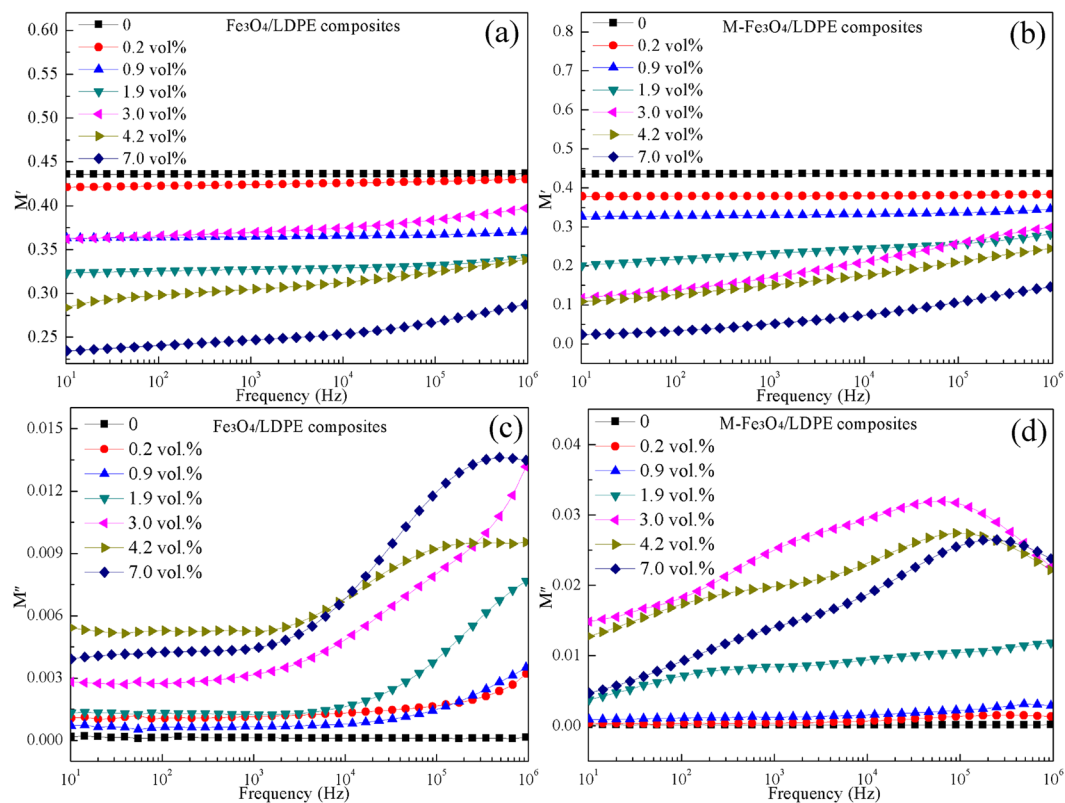


Figure 6. Frequency dependence of the (a,b) real parts and (c,d) imaginary parts of the complex electric modulus for the $\text{Fe}_3\text{O}_4/\text{LDPE}$ and $\text{M-Fe}_3\text{O}_4/\text{LDPE}$ composites.

Fe_3O_4 content (Fig. 6b), and increases with frequency; this behavior is similar to other polymer composites containing conducting fillers^{48,49}. As shown in Fig. 6c and d, compared with the $\text{Fe}_3\text{O}_4/\text{LDPE}$ composites, obvious interfacial polarization relaxation peaks occur for the $\text{M-Fe}_3\text{O}_4/\text{LDPE}$ composites when the Fe_3O_4 content is higher than 1.9 vol.%. Moreover, the relaxation strength of the composites decreases with the increase of Fe_3O_4 loading, and the relaxation peak moved toward higher frequency as the Fe_3O_4 content increased. The inter-particle distance would decrease as the volume fraction of the Fe_3O_4 increased, and as a result, the probability of Fe_3O_4 nanoparticles coming into contact increased because of the external magnetic field. As shown in Fig. 1d, some Fe_3O_4 particles come into contact with each other and become short chains along the direction of the magnetic field, which leads to a higher possibility for the charge carriers to accumulate on the interface between Fe_3O_4 and LDPE, the polarization and dielectric response are greatly enhanced under the electric field²². Therefore, a high dielectric constant of $\text{M-Fe}_3\text{O}_4/\text{LDPE}$ composites is achieved at a low volume fraction.

For polymer capacitors, it is essential that the dielectric properties of the composites retain excellent stability across a wide temperature range^{11,14}. In this research, the temperature dependence of the dielectric constant and dissipation factor of the $\text{Fe}_3\text{O}_4/\text{LDPE}$ and $\text{M-Fe}_3\text{O}_4/\text{LDPE}$ composites at 10 Hz are given in Fig. 7. It can be found that a minor variation in dielectric constant of the $\text{M-Fe}_3\text{O}_4/\text{LDPE}$ composites occurs with the increasing of temperature. The $\text{M-Fe}_3\text{O}_4/\text{LDPE}$ composites at 7.0 vol.% Fe_3O_4 concentration display the largest dielectric constant (>51) across the whole temperature ranges. However, for the $\text{Fe}_3\text{O}_4/\text{LDPE}$ composites, an obvious increasing trend occurred when the temperature was over 100 °C. Concurrently, the dissipation factor of the $\text{M-Fe}_3\text{O}_4/\text{LDPE}$ composites at 10 Hz also remained at a slightly low value and maintained good stability across the whole temperature range, but an appreciable change has been observed in the $\text{Fe}_3\text{O}_4/\text{LDPE}$ composites at 7.0 vol.% concentration. It is also evident that, of the dielectric assessed, the $\text{M-Fe}_3\text{O}_4/\text{LDPE}$ composites offer a stable dielectric constant and dissipation factor at high temperature. This is attributed to the fact that the higher thermal conductivity of the $\text{M-Fe}_3\text{O}_4/\text{LDPE}$ composites can effectively depress the dielectric loss and conductivity. It also indicates that the magnetic field could largely enhance the dielectric-temperature stability of the $\text{Fe}_3\text{O}_4/\text{LDPE}$ composites across broad temperature range. There is an undoubtable benefit to the use of $\text{Fe}_3\text{O}_4/\text{LDPE}$ composites across a wider temperature range in electronics.

In our present study, Fe_3O_4 nanoparticles adopted a directional arrangement along the direction of the magnetic field, and formed a conductive network in the LDPE matrix under the action of a magnetic field, resulting in greatly enhanced thermal conductivity. Moreover, the interfacial polarization of the $\text{Fe}_3\text{O}_4/\text{LDPE}$ composites is effectively enhanced under magnetic field treatment, and the maximum dielectric constant of the composites reaches 51 at 7.0 vol.% concentration. Additionally, the low volume fraction of the fillers and the excellent compatibility of the Fe_3O_4 nanoparticles and LDPE matrix, resulted in a relatively low dielectric loss (0.25) and a low conductivity (7×10^{-11} S/cm). Moreover, the dielectric properties of the $\text{M-Fe}_3\text{O}_4/\text{LDPE}$ composites retain

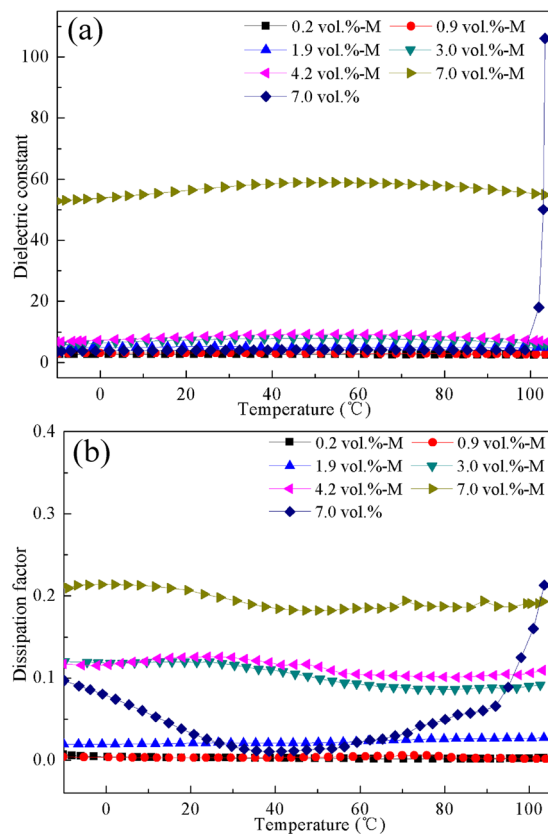


Figure 7. Temperature dependence of (a) dielectric constant and (b) dissipation factor of the $\text{Fe}_3\text{O}_4/\text{LDPE}$ and $\text{M-Fe}_3\text{O}_4/\text{LDPE}$ composites at different volume fraction of Fe_3O_4 filler at 10 Hz.

good stability across a wide temperature range (-10°C – 105°C), resulting from the high thermal conductivity of the $\text{Fe}_3\text{O}_4/\text{LDPE}$ composites induced by the magnetic field. This good heat dissipation capability prolonged the lifespan of the polymer dielectrics at a higher operating temperature.

Conclusion

In summary, Fe_3O_4 -deposited LDPE hybrid particles were prepared by a solvothermal reaction, and the corresponding $\text{Fe}_3\text{O}_4/\text{LDPE}$ composites were also prepared. SEM images show that Fe_3O_4 nanoparticles were embedded in the LDPE matrix without agglomeration and defects. The magnetic field enhanced the probability of forming Fe_3O_4 conductive chains, which can effectively enhance the heat flux and interfacial polarization of $\text{Fe}_3\text{O}_4/\text{LDPE}$ composites. The $\text{Fe}_3\text{O}_4/\text{LDPE}$ composites induced by the magnetic field exhibited higher thermal conductivity and a higher dielectric constant in comparison with the $\text{Fe}_3\text{O}_4/\text{LDPE}$ composites at the same filler content. Moreover, the relatively low dielectric loss and low conductivity are attributed to the low filler content and the improvement compatibility of the Fe_3O_4 nanoparticles and LDPE matrix by the surfactant treatment of the PDA. The low filler content leads to good mechanical properties and material processibility. Additionally, the dielectric properties of the $\text{M-Fe}_3\text{O}_4/\text{LDPE}$ composites also retain good stability across a wide temperature range, due to the high thermal conductivity of the $\text{Fe}_3\text{O}_4/\text{LDPE}$ composites induced by the magnetic field. This work establishes a facile, yet efficient approach to synthesize polymer materials with high thermal conductivity and high dielectric properties in order to make them suitable candidates for use in the electronics industry.

Materials and Methods

Preparation of Fe_3O_4 nanoparticles. The typical procedures for the preparation of the super-paramagnetic Fe_3O_4 nanoparticles were carried out as follows. Firstly, 1.442 g of $\text{FeSO}_4 \cdot 7\text{H}_2\text{O}$ and 2.472 g of $\text{FeCl}_3 \cdot 6\text{H}_2\text{O}$ were dissolved in 50 mL distilled water, respectively, then mixed together according to the mole ratio ($\text{Fe}^{3+}:\text{Fe}^{2+} = 2:1.134$) to inhibit the oxidation of Fe^{2+} . The iron solution and NaOH alkaline solution were slowly added to 100 mL distilled water in a 500 mL flask under vigorous stirring at 40°C for 30 min, the pH of aqueous solution in the whole process was fixed at 12–13. After standing for about 1 h, the precipitate was washed with distilled water and ethanol until the pH reached neutral. The Fe_3O_4 nanoparticles were obtained and dried under vacuum at 60°C for 12 h.

Preparation of Fe_3O_4 -LDPE particles. The typical procedures for the preparation of the super-paramagnetic Fe_3O_4 deposited on the LDPE particles (Fe_3O_4 -LDPE) were carried out as follows. Firstly, the desired amount of LDPE particles was poured into 175 ml ethanol, followed by the addition of Fe_3O_4 under

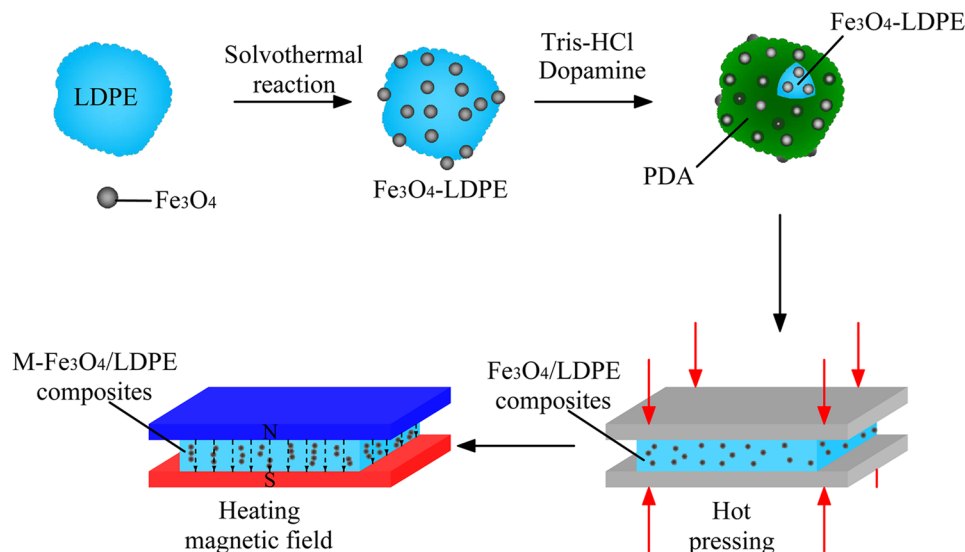


Figure 8. Schematic illustration of the preparation of the $\text{Fe}_3\text{O}_4/\text{LDPE}$ and $\text{M-Fe}_3\text{O}_4/\text{LDPE}$ composites.

vigorous stirring at room temperature for 15 min. Then, the obtained mixture was transferred into a 200 mL Teflon-lined stainless steel autoclave. The solvothermal reaction was kept at 120°C for 4 h, then the precipitate was collected, and washed with distilled water and ethanol until the pH around 7. Finally, the $\text{Fe}_3\text{O}_4/\text{LDPE}$ particles were obtained and dried under vacuum at 50°C for 12 h. The volume fractions of Fe_3O_4 in the $\text{Fe}_3\text{O}_4/\text{LDPE}$ particles were 0.2 vol.%, 0.9 vol.%, 1.9 vol.%, 3.0 vol.%, 4.2 vol.%, and 7.0 vol.%, respectively.

Preparation of $\text{Fe}_3\text{O}_4/\text{LDPE}$ composites. Before preparing the composites, the 0.6 g $\text{Fe}_3\text{O}_4/\text{LDPE}$ particles were dispersed in a 200 mL Tris-HCl aqueous solution (10×10^{-3} M, pH = 8.5) followed by sonication for 1 h; then 0.2 g DA-HCl was added and sonicated for another 10 min. The mixture was then stirred vigorously at room temperature for 4 h, and the excess supernatant was removed after sedimentation for about 1 h. The $\text{Fe}_3\text{O}_4/\text{LDPE}$ particles were obtained and dried under vacuum at 50°C for 12 h. The $\text{Fe}_3\text{O}_4/\text{LDPE}$ composites were obtained by a torque rheometer for 30 min at 130°C and then molded by hot pressing at approximately 130°C and 15 MPa for 20 min. The $\text{M-Fe}_3\text{O}_4/\text{LDPE}$ composites were obtained by treating at 130°C under a vertical direction magnetic field with a magnetic induction density of 1.0 T for 30 min. The preparation process of the $\text{Fe}_3\text{O}_4/\text{LDPE}$ and $\text{M-Fe}_3\text{O}_4/\text{LDPE}$ composites is shown in Fig. 8.

Characterization. The morphology of the $\text{Fe}_3\text{O}_4/\text{LDPE}$ particles and the microstructure of the LDPE composites were observed using SEM (Quanta 200 FEI). The phase compositions of the $\text{Fe}_3\text{O}_4/\text{LDPE}$ composites were analyzed using XRD (Empyrean), using $\text{Cu K}\alpha$ radiation at 40 kV and 40 mA. The thermal diffusivity (α) and specific heat (C) were measured on the disk samples with an LFA447 light flash system (NETZSCH, Selb, Germany) at 25°C . The thermal conductivity was calculated by $\lambda = \alpha C \rho$, in which ρ is the density of the $\text{Fe}_3\text{O}_4/\text{LDPE}$ composite. Prior to performing dielectric measurements, a layer of Al paste (diameter 25 mm) was evaporated on both surfaces to serve as electrodes. Dielectric measurements were employed across a frequency range from 10 to 10^6 Hz and a temperature range of -10°C to 105°C using a broad frequency dielectric spectrometer (Novocontrol Alpha-A).

References

- Zheng, M. S. *et al.* Enhanced breakdown strength of poly(vinylidene fluoride) utilizing rubber nanoparticles for energy storage application. *Appl. Phys. Lett.* **109**, 072902 (2016).
- Rocio, P. O., Antonio, F. & Marks, T. J. High-k organic, inorganic, and hybrid dielectrics for low-voltage organic field-effect transistors. *Chem. Rev.* **110**, 205–239 (2010).
- Chi, Q. G. *et al.* Effects of Zr doping on the microstructures and dielectric properties of $\text{CaCu}_3\text{Ti}_4\text{O}_{12}$ ceramics. *J. Alloy Compd.* **559**, 45–48 (2013).
- Dang, Z. M. *et al.* Fundamentals, processes and applications of high-permittivity polymer–matrix composites. *Prog. Mater. Sci.* **54**, 660–723 (2012).
- Zhang, C. H. *et al.* Enhanced dielectric properties of poly(vinylidene fluoride) composites filled with nano iron oxide-deposited barium titanate hybrid particles. *Sci. Rep.* **6**, 33508 (2016).
- Yang, W. H., Yu, S. H., Sun, R. & Du, D. X. Nano- and microsize effect of CCTO fillers on the dielectric behavior of CCTO/PVDF composites. *Acta Mater.* **59**, 5593–5602 (2011).
- Chi, Q. G. *et al.* Enhanced dielectric performance of amorphous calcium copper titanate/polyimide hybrid film. *J. Mater. Chem. C* **2**, 172–177 (2014).
- Luo, B. C., Wang, X. H., Wang, Y. P. & Li, L. T. Fabrication, characterization, properties and theoretical analysis of ceramic/PVDF composite flexible films with high dielectric constant and low dielectric loss. *J. Mater. Chem. A* **2**, 510–519 (2014).
- Dang, Z. M., Zheng, M. S. & Zha, J. W. 1D/2D Carbon Nanomaterial-Polymer Dielectric Composites with High Permittivity for Power Energy Storage Applications. *Small* **12**, 1688–1701 (2016).
- Wang, L. & Dang, Z. M. Carbon nanotube composites with high dielectric constant at low percolation threshold. *Appl. Phys. Lett.* **87**, 042903 (2005).

11. Li, Q. *et al.* Flexible high-temperature dielectric materials from polymer nanocomposites. *Nature* **523**, 576–579 (2015).
12. Zha, J. W. *et al.* Tuning of thermal and dielectric properties for epoxy composites filled with electrospun alumina fibers and graphene nanoplatelets through hybridization. *J. Mater. Chem. C* **3**, 7195–7202 (2015).
13. Schelling, P. K., Li, S. & Goodson, K. E. Managing heat for electronics. *Mater. Today* **8**, 30–35 (2005).
14. Zhou, W. Y. *et al.* Effect of the particle size of Al₂O₃ on the properties of filled heat-conductive silicone rubber. *J. Appl. Polym. Sci.* **104**, 1312–1318 (2007).
15. Luyt, A. S., Moldefi, J. A. & Krump, H. Thermal, mechanical and electrical properties of copper powder filled low-density and linear low-density polyethylene composites. *Polym. Degrad. Stabil.* **91**, 1629–1636 (2006).
16. Yang, Y., He, J. L., Wu, G. N. & Hu, J. “Thermal Stabilization Effect” of Al₂O₃ nano-dopants improves the high-temperature dielectric performance of polyimide. *Sci. Rep* **5**, 16986 (2015).
17. Min, C., Yu, D., Cao, J., Wang, G. & Feng, L. A graphite nanoplatelet/epoxy composite with high dielectric constant and high thermal conductivity. *Carbon* **55**, 116–125 (2013).
18. Ren, F., Ren, P. G., Di, Y. Y., Chen, D. M. & Liu, G. G. Thermal, Mechanical and Electrical Properties of Linear Low-Density Polyethylene Composites Filled with Different Dimensional SiC Particles. *Polym. Plast. Technol* **50**, 791–796 (2011).
19. Zeng, J. L. *et al.* Effects of MWNTs on phase change enthalpy and thermal conductivity of a solid-liquid organic PCM. *J. Therm. Anal. Calorim.* **95**, 507–512 (2009).
20. Yuan, C. *et al.* Thermal Conductivity of Polymer-Based Composites with Magnetic Aligned Hexagonal Boron Nitride Platelets. *ACS Appl. Mater. Interfaces* **7**, 13000–13006 (2015).
21. Li, W. P., Yu, L. J., Zhu, Y. J. & Hua, D. Y. External Magnetic Field Induced Percolation in Polyvinylidene Fluoride and Nickel Composites. *J. Phys. Chem. C* **114**, 14004–14007 (2010).
22. Chi, Q. G. *et al.* Nano iron oxide-deposited calcium copper titanate/polyimide hybrid films induced by an external magnetic field: toward a high dielectric constant and suppressed loss. *J. Mater. Chem. C* **4**, 8179–8188 (2016).
23. Yang, K., Huang, X. Y., He, J. L. & Jiang, P. K. Strawberry-like Core-Shell Ag@Polydopamine@BaTiO₃ Hybrid Nanoparticles for High-*k* Polymer Nanocomposites with High Energy Density and Low Dielectric Loss. *Adv. Mater. Interfaces* **2**, 1500361 (2015).
24. Li, Y. *et al.* Large Dielectric Constant and High Thermal Conductivity in Poly(vinylidene fluoride)/Barium Titanate/Silicon Carbide Three-Phase Nanocomposites. *ACS Appl. Mater. Interfaces* **3**, 4396–4403 (2011).
25. Jin, W. Q., Yuan, L., Liang, G. Z. & Gu, J. Multifunctional cyclotriphosphazene/hexagonal boron nitride hybrids and their flame retarding bismaleimide resins with high thermal conductivity and thermal stability. *ACS Appl. Mater. Interfaces* **6**, 14931–14944 (2014).
26. Lee, G. W., Park, M., Kim, J. Y., Lee, J. I. & Yoon, H. G. Enhanced thermal conductivity of polymer composites filled with hybrid filler. *Compos. Part A-Appl. S* **37**, 727–734 (2006).
27. Baglari, S., Kole, M. & Dey, T. K. Effective thermal conductivity and coefficient of linear thermal expansion of high-density polyethylene-flyash composites. *Indian J. Phys.* **85**, 559–573 (2011).
28. Xie, S. H., Zhu, B. K., Li, J. B., Wei, X. Z. & Xu, Z. K. Preparation and properties of polyimide/aluminum nitride composites. *Polym Test* **23**, 797–801 (2004).
29. Lin, Z. Y. *et al.* Magnetic alignment of hexagonal boron nitride platelets in polymer matrix: toward high performance anisotropic polymer composites for electronic encapsulation. *ACS Appl. Mater. Interfaces* **5**, 7633–7640 (2013).
30. Su, N. C., Smith, Z. P., Freeman, B. D. & Singh, J. J. Size-Dependent Permeability Deviations from Maxwell’s Model in Hybrid Cross-Linked Poly(ethylene glycol)/Silica Nanoparticle Membranes. *Chem. Mater.* **27**, 2421–2429 (2015).
31. Shen, M. X., Cui, Y. X. & He, J. Thermal conductivity model of filled polymer composites. *International Journal of Minerals Metallurgy & Materials. Int. J. Min. Met. Mater.* **18**, 623–631 (2011).
32. Agari, Y. & Uno, T. Estimation on Thermal Conductivities of Filled Polymers. *J. Appl. Polym. Sci.* **32**, 5705–5712 (2003).
33. Agari, Y., Tanaka, M., Nagai, S. & Uno, T. Thermal conductivity of a polymer composite filled with mixtures of particles. *J. Appl. Polym. Sci.* **34**, 1429–1437 (1987).
34. Zhou, Y. C. *et al.* The use of polyimide-modified aluminum nitride fillers in AlN@PI/epoxy composites with enhanced thermal conductivity for electronic encapsulation. *Sci. Rep* **4**, 4779 (2014).
35. Agari, Y., Ueda, A., Tanaka, M. & Nagai, S. Thermal Conductivity of a Polymer Filled with Particles in the Wide Range From Low to Super-high Volume Content. *J. Appl. Polym. Sci.* **5**, 929–941 (1990).
36. Florian, E. & Thomas, T. A. Controlling the Orientation of Semicrystalline Polymers by Crystallization in Magnetic Fields. *Macromolecules* **36**, 8685–8694 (2003).
37. Tsunehisa, K. Study on the Effect of Magnetic Fields on Polymeric Materials and Its Application. *Polym. J.* **35**, 823–843 (2003).
38. Vilens’kyi, V. O. & Demchenko, V. L. Influence of the intensity of constant magnetic field on the structure and properties of composites based on epoxy polymers and Fe (III) or Al(III) oxides. *Mater. Sci* **45**, 409–416 (2009).
39. Wang, G. Enhanced dielectric properties of three-phase-percolative composites based on thermoplastic-ceramic matrix (BaTiO₃ + PVDF) and ZnO radial nanostructures. *ACS Appl. Mater. Interfaces* **2**, 1290–1293 (2010).
40. Xie, L. Y., Huang, X. Y., Huang, Y. H., Yang, K. & Jiang, P. K. Core-shell structured hyperbranched aromatic polyamide/BaTiO₃ hybrid filler for poly (vinylidene fluoride-trifluoroethylene-chlorofluoroethylene) nanocomposites with the dielectric constant comparable to that of percolative composites. *ACS Appl. Mater. Interfaces* **5**, 1747–1756 (2013).
41. Yang, Y. *et al.* High performance of polyimide/CaCu₃Ti₄O₁₂@Ag hybrid films with enhanced dielectric permittivity and low dielectric loss. *J. Mater. Chem. A* **3**, 4916–4921 (2015).
42. Ramani, R. *et al.* A Free Volume Study on the Origin of Dielectric Constant in a Fluorine-Containing Polyimide Blend: Poly(vinylidene fluoride-co-hexafluoro propylene)/Poly(ether imide). *J. Phys. Chem. B* **118**, 12282–12296 (2014).
43. Chi, Q. G. *et al.* Effect of particle size on the dielectric properties of 0.5Ba(Zr_{0.2}Ti_{0.8})O₃-0.5(Ba_{0.7}Ca_{0.3})TiO₃/polyvinylidene fluoride hybrid films. *Ceram. Int.* **41**, 15446–15121 (2015).
44. Sun, W. X. *et al.* Multifunctional Properties of Cyanate Ester Composites with SiO₂ Coated Fe₃O₄ Fillers. *ACS Appl. Mater. Interfaces* **5**, 1636–1642 (2013).
45. Zhu, J. J. *et al.* An ultrahigh dielectric constant composite based on polyvinylidene fluoride and polyethylene glycol modified ferroferric oxide. *J. Phys. D: Appl. Phys* **48**, 355301 (2015).
46. Havriliak, S. & Negami, S. A. Complex Plane Representation of Dielectric and Mechanical Relaxation Processes in Some Polymers. *Polymer* **8**, 161–210 (1967).
47. Yang, W. H. *et al.* Electrical modulus analysis on the Ni/CCTO/PVDF system near the percolation threshold. *J. Phys. D:Appl. Phys* **44**, 475305–475312 (2011).
48. Laurati, M. *et al.* Dynamics of Water Absorbed in Polyamides. *Macromolecules* **45**, 1676–1687 (2012).
49. Huang, X. Y. *et al.* Temperature-dependent electrical property transition of graphene oxide paper. *Nanotechnology* **23**, 1–8 (2012).

Acknowledgements

The authors thanks the support of the National Science Foundation of China (61640019), the Open Foundation of State Key Laboratory of Electronic Thin Films and Integrated Devices (KFJJ201601), Science Funds for the Young Innovative Talents of HUST (201102).

Author Contributions

The research was planned by Q.G.C.; Experiments were performed by T.M. and J.F.D.; Q.G.C. and T.M. prepared the manuscript; Y.C. and Y.Z. prepared figures in all paper; C.H.Z. and Q.G.C. analyzed the results; S.C.X., X.W. and Q.Q.L. checked the scientific information and flow of the text to maintain a better readability; All the authors participated in discussing and reviewing of the manuscript.

Additional Information

Competing Interests: The authors declare that they have no competing interests.

Publisher's note: Springer Nature remains neutral with regard to jurisdictional claims in published maps and institutional affiliations.



Open Access This article is licensed under a Creative Commons Attribution 4.0 International License, which permits use, sharing, adaptation, distribution and reproduction in any medium or format, as long as you give appropriate credit to the original author(s) and the source, provide a link to the Creative Commons license, and indicate if changes were made. The images or other third party material in this article are included in the article's Creative Commons license, unless indicated otherwise in a credit line to the material. If material is not included in the article's Creative Commons license and your intended use is not permitted by statutory regulation or exceeds the permitted use, you will need to obtain permission directly from the copyright holder. To view a copy of this license, visit <http://creativecommons.org/licenses/by/4.0/>.

© The Author(s) 2017